Laurentide Ice Sheet thinning and erosive regimes at Mount Washington, New Hampshire, inferred from multiple cosmogenic nuclides

Alexandria J. Koester[1,2] *, Jeremy D. Shakun[1], Paul R. Bierman[3], P. Thompson Davis[4], Lee B. Corbett[3], Brent M. Goehring[5], Anthony C. Vickers[1], Susan R. Zimmerman[6]

[1]Department of Earth and Environmental Sciences, Boston College, Chestnut Hill, MA 02467

[2]Department of Earth, Atmospheric, and Planetary Sciences, Purdue University, West Lafayette, IN 47907

[3]Department of Geology, University of Vermont, Burlington, VT 05405

[4]Department of Natural and Applied Sciences, Bentley University, Waltham, MA 02452

[5]Department of Earth and Environmental Sciences, Tulane University, New Orleans, LA 70118

[6]Center for Accelerator Mass Spectrometry, Lawrence Livermore National Laboratory, Livermore, CA 94550

*Corresponding author. Email: koestea@purdue.edu (A. J. Koester)

ABSTRACT

The northward retreat history of the Laurentide Ice Sheet through the lowlands of the northeastern United States during the last deglaciation is well constrained, but its vertical thinning history is less well known because of the lack of direct constraints on ice thickness through time and space. In addition, the highest elevations in New England are characterized by gently sloping upland surfaces and weathered blockfields, features with an uncertain history. To better constrain ice sheet history in this area and its relationship to alpine geomorphology, we present 20 new ^{10}Be and seven in-situ ^{14}C cosmogenic nuclide measurements along an elevation transect at Mount Washington, New Hampshire, the highest mountain in the northeastern United States (1917 m a.s.l.). Our results suggest substantially different exposure and erosion histories on the upper and lower parts of the mountain. Above 1600 m a.s.l., ^{10}Be and in-situ ^{14}C measurements are consistent with upper reaches of the mountain deglaciating by 18 ka. However, some

^{10}Be ages are up to several times greater than the age of the last deglaciation, consistent with weakly erosive, cold-based ice that did not deeply erode pre-glacial surfaces. Below 1600 m a.s.l., ^{10}Be ages are indistinguishable over a nearly 900-m range in elevation and imply rapid ice-surface lowering about 14.1 ± 1.1 ka (n = 9, 1SD). This shift from slow thinning early in the deglaciation on the upper part of the mountain to abrupt thinning across the lower elevations coincides with accelerated ice-margin retreat through the region recorded by Connecticut River valley varve records during the Bølling Interstadial (Ridge et al., 2012). The Mount Washington cosmogenic nuclide vertical transect and the Connecticut River valley varve record, along with other New England cosmogenic nuclide records, suggest rapid ice-volume loss in interior northeastern United States in response to Bølling warming.

INTRODUCTION AND BACKGROUND

The deglacial history of New England (northeastern United States) can provide valuable information on ice-sheet thinning dynamics during rapid climate changes. The area was covered by the southeastern sector of the Laurentide Ice Sheet (LIS), the largest Northern Hemisphere ice sheet during the Last Glacial Maximum (LGM). Deglaciation of the area spanned several abrupt climate events centered in the North Atlantic (Ridge et al., 2012) and the LIS covered mountainous terrain, which provides an opportunity to reconstruct the history of interior ice-sheet thinning that can be linked with well-constrained records of marginal retreat.

We measured a vertical transect of cosmogenic nuclide ages on 20 boulder and bedrock samples from Mount Washington in the Presidential Range of New Hampshire's White Mountains, the tallest peak in the northeastern United States (1917 m a.s.l.), to address the following questions. Was the summit of Mount Washington ice-covered during the LGM? If so, when, and for how long? When, and how rapidly, did continental ice at Mount Washington thin during the last deglaciation?

Laurentide Ice Sheet History in New England

Direct evidence of pre-LGM ice-sheet history in New England is sparse, but previous research suggests a single advance into the region during the last glacial cycle following rapid growth of the LIS during late Marine Isotope Stage (MIS) 3 (Carlson et al., 2018; Batchelor et al., 2019). An earlier till beneath MIS 2 till in this area is likely MIS 6 in age or older, though an MIS 4 age cannot be ruled out (Clark et al., 1993). Pre-LGM sediments suggest that the St. Lawrence lowlands just north of New England were ice-free at ~37.5 (Parent and Dubé-Loubert, 2017). Similarly, cave sediments in Vermont and lake sediments in Maine preclude ice advance across the St. Lawrence until after 35 ka (Anderson et al., 1986; Munroe et al., 2016). High relative sea levels along the U.S. mid-Atlantic coast require a restricted LIS and reduced forebulge in eastern North America before 35 ka (Pico et al., 2017). Lastly, glacial-isostatic adjustment modeling suggests that eastward diversion of the Hudson River at ~30 ka is attributable to rapid, late growth of the LIS in this region (Pico et al., 2018). While these regional constraints suggest that continental ice did not advance into New England until MIS 2, it is possible that local ice domes formed during the pre-LGM period over the Appalachian highlands, perhaps later coalescing with the expanding LIS (Flint, 1951; Dredge and Thorleifson, 1987). Furthermore, unweathered summit erratics indicate that the LIS overtopped the Presidential Range at some point during the Pleistocene (Goldthwait, 1916; Antevs, 1932; Goldthwait, 1940, 1970a), but it is unclear if this overtopping occurred during the most recent glacial cycle due to a lack of dating constraints.

The marginal retreat of the LIS through time is constrained in New England by minimum-limiting radiocarbon ages (e.g., Dyke, 2004; Peteet et al., 2012), glacial varve chronologies (e.g., Ridge et al., 2012), and cosmogenic nuclide dating in an increasing number of locations (Fig. 1 and references therein). The LIS began retreating from its maximum extent by ~25 ka based on ^{10}Be ages of terminal moraines from Martha's Vineyard, Massachusetts (27.5 ± 2.2 ka) (Balco et al., 2002) and northern New Jersey (25.2 ± 2.1 ka) (Corbett et al., 2017) (Fig. 1) (all ^{10}Be ages reported in this manuscript have been recalculated with the northeastern North American production rate calibration dataset [Balco et al., 2009] and LSDn scaling [Lifton et al., 2014)]). Initial retreat was limited to <100 km for the next several millennia after ~25 ka, reaching Buzzards Bay, Massachusetts (20.3 ± 1.2 ka) (Balco et al., 2002), and

Old Saybrook and Ledyard, Connecticut (20.7 ± 0.9 ka and 20.7 ± 0.7 ka) (Balco and Schaefer, 2006) moraines at ~20 ka. The North American Varve Chronology outlines a high-resolution record of ice margin retreat up the length of the Connecticut River valley (Ridge et al., 2012). This record suggests that ice retreated gradually at 30–100 m yr^{-1} from ~19 to 15 ka, depositing the North Charlestown moraines across central New England just before the Bølling warming at 14.6 ka. Coastal Maine, mostly below the marine limit, also deglaciated around this time, with ^{10}Be ages from Acadia National Park and the Pineo Ridge moraine complex centered on ~15 ka (Koester et al., 2017; Hall et al., 2017). Subsequently, the rate of lateral retreat increased dramatically to ~300 m yr^{-1} in the Connecticut River valley, retreating north of the latitude of Mount Washington at ~14.2 ka (Ridge et al., 2012). The LIS margin readvanced briefly during the Older Dryas cooling event to deposit the Littleton-Bethlehem, Berlin, and Androscoggin moraines across the northern flank of the White Mountains 14.0–13.7 ka (Balco et al., 2009; Thompson et al., 2017; Bromley et al., 2015, 2019) and retreated into southern Quebec by ~13.5 ka (Dyke, 2004; Ridge et al., 2012).

In contrast to the ice margin retreat history, the timing and pace of LIS thinning in New England is more ambiguous. LIS retreat at higher elevations in New England is constrained by minimum-limiting radiocarbon ages from alpine lakes, though they exhibit inconsistencies, some ages suggesting a pattern opposite that expected from top-down deglaciation (Davis et al., 2017). For instance, a basal bulk radiocarbon age of 13.2–13.5 cal. ka (11.5 ± 0.2 ^{14}C ka BP) from the lower Lakes of the Clouds (1534 m a.s.l.) just below the Mount Washington summit is younger than an analogous basal bulk age of 14.7–16.0 cal. ka (12.9 ± 0.4 ^{14}C ka BP) from Lost Pond (625 m a.s.l.) at the foot of the mountain (Spear, 1989; Spear et al., 1994; Cwynar and Spear, 2001) (all radiocarbon ages are recalibrated with Calib v. 7.10 [Stuiver et al., 2015] using the IntCal13 calibration curve [Reimer et al., 2013]). In addition, basal radiocarbon ages of 11.5–12.9 cal. ka (10.5 ± 0.5 ^{14}C ka BP) and 11.8–13.0 cal. ka (10.7 ± 0.04 ^{14}C ka BP) from Lonesome Lake (831 m a.s.l.) and Profile Lake (593 m a.s.l.) in Franconia Notch (Spear et al, 1994; Rogers, 2003) are significantly younger than the pond-bottom radiocarbon ages from Mount

Washington just to the east. In sum, pond- and bog-bottom radiocarbon ages are not useful for precisely defining ice thinning history in the alpine terrain of New England (Davis and Davis, 1980).

More recently, cosmogenic nuclide measurements on a few New England mountains were used to constrain ice-sheet thinning histories directly. Many of these cosmogenic nuclide ages, particularly at lower elevations, are interpreted to accurately record deglacial timing, and suggest that the LIS thinned rapidly at Katahdin, Maine, between 16 and 15 ka (Davis et al., 2015), Mount Mansfield, Vermont, at 13.9 ± 0.6 ka (Corbett et al., 2019), and the Adirondack Mountains, New York, between 16 and 13 ka (Barth et al., 2019) (Fig. 1). However, numerous cosmogenic nuclide ages from higher on these peaks, as well as from the summits of Mount Washington and Little Haystack, New Hampshire (Bierman et al., 2015), are substantially older than the regional deglaciation age. These data have been interpreted as implying that the LIS was largely cold-based at high elevations in New England and thus insufficiently erosive to remove nuclides inherited from pre-LGM exposure (Bierman et al., 2015; Corbett et al., 2019). It is also possible that some of these older ages reflect early ice-sheet thinning before deglaciation of the lowlands (Barth et al., 2019) and/or that the highest summits remained exposed as nunataks throughout the last glaciation (e.g., Fernald, 1925).

Presidential Range Geomorphology

Periglacial features that dominate the upper elevations of the Presidential Range were recognized by Antevs (1932), although their age and relation to glaciation remains unclear (Fig. 2) (Fowler et al., 2013). Summits in the Presidential Range are mantled by weathered blockfields of large (>1 m), angular, frost-riven blocks covered in lichens and underlain by clay-rich till (Goldthwait, 1970a) and 30-m thick permafrost (e.g., Pewe, 1983). These blockfields may have formed before the last glaciation and either remained exposed through the LGM on summit nunataks or were preserved under cold-based ice cover (e.g., Clark and Schmidlin, 1992). Alternatively, the blockfields could be in part products of postglacial weathering (Goldthwait et al., 1987). Below the level of the blockfields on summits are gently sloping areas known as “lawns” (e.g., Bigelow Lawn, the Alpine Garden, and Monticello Lawn), which together

make up a topographic feature called the Presidential Upland (Goldthwait, 1940). The lawns are interpreted to be either a pre-Quaternary erosion surface formed during a prolonged lull in tectonic uplift (Goldthwait, 1940; Eusden and Fowler, 2013) or the result of freeze-thaw processes during the Quaternary (Thompson, 1960, 1961a, 1961b). The surfaces of the lawns are covered in patterned ground, including inactive large-scale block nets, stripes, and lobes, as well as miniature periglacial features still active today (Goldthwait et al., 1987; Clark and Schmidlin, 1992).

In contrast to the relatively subdued and weathered landscapes above ~1600 m a.s.l., the lower elevations of the Presidential Range are clearly modified by glacial erosion. Numerous cirques on the eastern flank of the range were occupied by local glaciers prior to LIS advance into New England (J.W. Goldthwait, 1913, 1916; R.P. Goldthwait, 1970b; Davis, 1988, 1999), while Pinkham Notch (~650 m a.s.l.) at the base of Mount Washington's eastern side is one of several deep, north-south oriented U-shaped valleys scoured by the LIS in the White Mountains.

Farther north and across the Atlantic Ocean, other alpine environments with trimlines separating high-elevation blockfields from glacially scoured lower slopes have been the subject of similar inquiry regarding whether the mountaintops remained exposed as nunataks during the LGM. Cosmogenic nuclide dating of boulders and bedrock across elevation transects has helped resolve these debates in parts of Canada (e.g., Marsella et al., 2000; Marquette et al., 2004; Briner et al., 2006), the British Isles (e.g., Fabel et al., 2012; Ballantyne and Stone, 2015), and Scandinavia (e.g., Brook et al., 1996; Goehring et al., 2008; Gjermundsen et al., 2015), suggesting that these trimlines mark the upper limits of glacial erosion instead of the upper limits of ice extent. These trimlines represent a former englacial thermal boundary between a lower zone of warm-based sliding ice and an upper zone of cold-based ice frozen to the bed.

METHODS

Cosmogenic Nuclides

Given the possibility that cold-based ice did not deeply erode rock surfaces and remove nuclides from earlier periods of exposure on the upper flanks of on Mount Washington, we measured both long-

lived ^{10}Be and short-lived ^{14}C , because the nuclide concentrations can reflect different timescales of a once-glaciated surface's history (Gosse and Phillips, 2001). With its long half-life, ^{10}Be experiences minimal decay on the time scale of 100 kyr glacial cycles ($t_{1/2}$=1.39 Myr; Chmeleff et al., 2010; Korschinek et al., 2010) and thus can preserve exposure from previous interglacials. In contrast, in-situ ^{14}C is mostly removed by decay within ~25 kyr ($t_{1/2}$=5.7 kyr). The concentration of in-situ ^{14}C is therefore less affected by pre-LGM exposure and resulting nuclide inheritance, and has the potential to be a more faithful chronometer of recent deglaciation (Goehring et al., 2019a). In-situ ^{14}C concentrations asymptotically approach saturation, with production matched by decay, after ~25 kyr of exposure, and therefore only provide minimum limiting exposure ages beyond ~25 ka.

Sampling

We collected samples from 20 rock surfaces (9 bedrock and 11 boulders) for in-situ cosmogenic nuclide analysis along a transect from the summit of Mount Washington to Pinkham Notch (1907 to 656 m a.s.l.), a vertical range of 1251 m (Fig. 2, 3; Table 1) – all of these were analyzed for ^{10}Be. Five of the bedrock samples are from in-situ bedrock, while four samples are from frost-riven blocks–jointed angular bedrock blocks that have likely moved through frost action. Boulders are sub-rounded to sub-angular and typically perched on bedrock. All samples are composed of the local schist bedrock. In seven of these 20 samples we also measured in-situ ^{14}C; two frost-riven summit blocks (MW-22, MW-23) and a boulder just below the summit (MW-05), a boulder and rôche moutonnée from Bigelow Lawn (MW-01, MW-02), and boulder and bedrock samples from a bench about halfway down the mountain (MW-13, MW-15).

Where possible, we targeted surfaces that exhibited characteristics of glacial erosion, such as polish (MW-07, MW-13), grooves (MW-08), molding (MW-09, MW-19), and rôche moutonnées (MW-01, MW-13), to reduce the likelihood of measuring ^{10}Be inherited from prior episodes of exposure and to minimize the likelihood of postglacial erosion of these surfaces. We also sampled boulders away from slopes to reduce the probability of postglacial movement (MW-02, MW-05, MW-11, MW-14, MW-15),

and we avoided bedrock with signs of soil cover or till within several meters of sample sites. Higher elevations are frequently windswept, and the summit is covered by 12 cm of snow averaged across the year based on a 20-year record (1995-2015) (T. Padham, personal communication, 2017). Thus snow burial would lower ^{10}Be ages <2 %, well within our reported uncertainty. Although a thicker snow pack is possible elsewhere on the mountain and at times in the past, most of our samples are from exposed ridgelines that are more likely to be windswept and nearly all of our boulders are 1–2 m high (Table 1). We recorded location and elevation with a handheld GPS, measured topographic shielding using a clinometer, determined surface orientation with a Brunton compass, measured boulder heights and sample thicknesses, and photographed sample sites.

Nuclide Extraction and Measurement

Quartz was isolated from the samples at the University of Vermont. Samples were crushed, sieved to 250–800 μm, magnetically separated, feldspars and micas removed via froth flotation (Nichols and Goehring, 2019), and etched in dilute hydrofluoric acid to remove remaining non-quartz phases and any meteoric ^{10}Be (Kohl and Nishiizumi, 1992). Quartz purity was measured with inductively coupled plasma optical-emission spectrometry.

Beryllium was extracted at the University of Vermont Cosmogenic Nuclide Laboratory following the methods described in Corbett et al. (2016). About 250 μg of ^{9}Be (carrier made from beryl at University of Vermont) was added to each sample before digestion. Samples were prepared in three batches, each containing one CRONUS standard (Standard N; Jull et al., 2015) and one process blank. Beryllium was isolated through anion and cation column chromatography, precipitated as a hydroxide gel, calcinated, mixed with niobium powder, and pressed into cathodes for measurement. ^{10}Be/^{9}Be ratios were measured at Lawrence Livermore National Laboratory relative to materials prepared by Kuni Nishiizumi (standard 07KNSTD3110) with an assumed ^{10}Be/^{9}Be ratio of 2850 x 10^{-15} (Nishiizumi et al., 2007). We corrected for backgrounds by subtracting the average of four process blanks (1.08 ± 0.46 x 10^{-15}, 1 standard deviation (SD)) from all sample values and propagated uncertainties in quadrature. Blank-

corrected $^{10}Be/^{9}Be$ ratios range from 9.70 x 10^{-14} to 2.11 x 10^{-12} and analytical uncertainties (including the propagated blank uncertainty) are 2.3 ± 0.6 % (mean, 1SD; Supplemental Table S1).

Carbon was extracted at Tulane University following the methods of Goehring et al. (2019b). Samples were heated at 500 °C in high-purity O_2 to remove atmospheric contaminants, subsequently heated to 1100 °C where the quartz was fused via $LiBO_2$, oxidized to CO_2 in a high-purity O_2 atmosphere, and cryogenically collected. The samples were purified and converted to filamentous graphite for AMS measurement. $^{14}C/^{13}C$ ratios were measured relative to Oxalic acid II (NIST-4990C) at Lawrence Livermore National Laboratory and the National Ocean Sciences Accelerator Mass Spectrometry facility. Stable carbon isotope ratios were measured via isotope ratio mass spectrometry at the UC-Davis Stable Isotope Facility. Measured ^{14}C atoms were calculated from the $^{14}C/C_{total}$ and blank-corrected by subtracting the effective blank (in atoms) associated with extraction. Blank-corrected ^{14}C concentrations range from 5.31 x 10^5 to 2.45 x 10^5 atoms g^{-1} and reported analytical uncertainties range from 3.88 x 10^3 to 7.10 x 10^3 atoms g^{-1} (Supplemental Table S2). However, rather than use this narrower estimate of analytical precision, we report ^{14}C data with a more conservative estimate of long-term lab precision (5.6%; Goehring et al., 2019b) based on replicate measurements of the CRONUS-A intercomparison material (Jull et al., 2015).

Cosmogenic Nuclide Age Calculations

Cosmogenic nuclide ages were calculated with version 3 of the online University of Washington cosmogenic calculators (wrapper script: 3.0.2, constants: 3.0.4, muons: 1A, Balco et al., 2008), using the northeastern North American production rate calibration dataset for ^{10}Be and ^{14}C production rate derived from measurements of CRONUS-A, which was collected from an Antarctic surface saturated with respect to ^{14}C (Balco et al., 2009; Goehring et al., 2019b). We use LSDn scaling because it accounts for nuclide-specific differences in production of ^{10}Be and ^{14}C (Lifton et al., 2014; Borchers et al., 2016; Lifton et al., 2016). Given our estimated ^{14}C analytical precision (5.6%), as well as ^{14}C production rate uncertainty (5.6%; Goehring et al., 2019b), concentrations are indistinguishable from saturation after 21 kyr of

exposure at 1σ uncertainty or 15 kyr of exposure at 2σ uncertainty (Fig. 4). We recalculated the five ^{10}Be ages and one in-situ ^{14}C age reported by Bierman et al. (2015) from the summit of Mount Washington using the same production and scaling parameters as above and include them in our discussion (Supplemental Table S3). This recalculation shifts ^{10}Be ages ~7% younger compared to the Lal (1991)/Stone (2000) time invariant scaling Bierman et al. (2015) used, and the ^{14}C age they reported becomes ~5 kyr older. Ages discussed below report 1σ external (i.e., analytical and production rate) uncertainties to facilitate comparison with records based on other chronometers (e.g., varves and radiocarbon).

RESULTS

If we assume all nuclides accumulated during a single period of exposure, the ^{10}Be ages range from 12.5 ± 1.1 to 77.1 ± 6.7 ka (Table 2) and generally show a strong ordering with elevation (Figs. 3, 5). ^{10}Be ages below ~1600 m a.s.l. are similar to each other and cluster around 14 ka (except for bedrock sample MW-13, 32.0 ± 2.8 ka). Above ~1600 m a.s.l., the cosmogenic nuclide ages are increasingly scattered and older near the summit, reaching values several times higher than the lowland deglaciation age. For example, a bedrock sample (MW-09) and rôche moutonnée (MW-01) on the lawns have ^{10}Be ages of 18.8 ± 1.6 and 74.5 ± 6.6 ka, respectively, whereas the two frost-riven summit blocks (MW-23, 46.6 ± 4.1; MW-22, 77.1 ± 6.7 ka) fall in the age range of Mount Washington summit samples reported by Bierman et al. (2015), 16.4 ± 1.9 to 137.4 ± 12.1 ka. The old ages at high elevations are derived from boulder and bedrock samples; two-meter-tall boulders on Bigelow Lawn (MW-02) and immediately off the summit (MW-05) have ^{10}Be ages of 31.8 ± 2.7 and 34.3 ± 3.0 ka.

In-situ ^{14}C ages are ordered by elevation as are the ^{10}Be ages (Table 2). All ^{14}C concentrations that we measured above 1600 m a.s.l. are saturated within uncertainty, while two samples at 1370 m a.s.l. have younger ^{14}C ages of 11.3 ± 1.8 ka and 15.6 ± 3.5 ka (Fig. 3, 4). However, Bierman et al.'s (2015) summit ^{14}C age (17.9 ± 3.5 ka) is slightly younger than our summit ^{14}C ages (Fig. 4). All samples in

which $^{14}C/^{10}Be$ ratios were measured are consistent with continuous exposure, though the high elevation samples could permit brief cover up to ~1 kyr (Fig. 6).

DISCUSSION

The Summit and Lawns: Cold-based Ice Cover and Early Deglaciation

The scattered and relatively old ^{10}Be ages above 1600 m a.s.l. point to a complex exposure-erosion history on the Mount Washington lawns and summit cone with some ^{10}Be ages predating the LGM. Similar patterns are observed in other glaciated areas at higher latitudes (Brook et al., 1996; Marsella et al., 2000; Marquette et al., 2004; Briner et al., 2006; Goehring et al., 2008; Fabel et al., 2012; Corbett et al., 2013; Gjermundsen et al., 2015; Winsor et al., 2015). These studies attribute old ^{10}Be ages and weathered landscapes at higher elevations to preservation of pre-LGM surfaces under weakly erosive, predominately cold-based ice cover. We likewise suggest that the ^{10}Be ages above 1600 m a.s.l. on Mount Washington, coupled with the preservation of summit blockfields and gently sloping lawns, reflect minimal erosion by ice that was, at least in part, cold-based.

The calculated cosmogenic ages are not indicative of constant exposure. If the summit of Mount Washington had remained exposed throughout the last glacial cycle, and sampled surfaces had not eroded or been covered by soil or till, cosmogenic nuclide ages would record >100 kyr exposure. Instead, nearly all ^{10}Be ages above 1600 m a.s.l. are ~20–80 ka (Fig. 3, 5). Some of the ^{10}Be age scatter among blockfield samples (39.9 ± 3.5 to 137.4 ± 12.1 ka) could reflect differences in the exposure durations of sampled block surfaces as blocks were churned through time by frost action. The spread of ages among large glacially derived boulders (22.0 ± 1.9 to 34.3 ± 3.0 ka) and bedrock (16.4 ± 1.4 to 74.5 ± 6.6 ka) samples, however, likely reflects spatially variable erosion under LGM ice cover. We cannot differentiate whether this ice cover was from a local ice cap or the LIS because these boulders all are composed of local bedrock.

Ice–margin constraints from the surrounding lowlands limit the timing of summit ice cover (if it was from the LIS) to a relatively brief interval during the LGM. Numerous data suggest that the LIS did

not extend into New England until after ~35 ka (Parent and Dubé-Loubert, 2017; Munroe et al., 2016; Pico et al., 2017, 2018), perhaps advancing in association with the rapid drop of global sea level toward the LGM lowstand at the onset of Marine Isotope Stage 2 at ~30 ka (Lambeck et al., 2014). Ice subsequently withdrew from the valleys around Mount Washington by ~14 ka (Dyke, 2004; Balco et al., 2009; Ridge et al., 2012; Bromley et al., 2015, 2019). Thus the LIS covered Mount Washington for at most ~15 kyr, and perhaps substantially less given the time required for ice to thicken over the topography.

Our ^{10}Be and ^{14}C ages may help to further constrain the time interval of summit ice cover. If we consider the molded bedrock surfaces above 1600 m a.s.l. with the youngest ^{10}Be ages (16.4 ± 1.4 to 18.8 ± 1.6 ka) to be the most deeply eroded by LGM ice, they provide a maximum-limiting deglaciation age of ~18 ka (Fig. 3, 5), presuming no post-exposure erosion and/or cover. In-situ ^{14}C would be expected to yield a similar or younger deglacial timing because it is less sensitive to pre-LGM nuclide inheritance, but the five ^{14}C samples we measured above 1600 m a.s.l. are within error of saturation and collectively suggest total exposure of >21 ka (Fig. 4).

Both ^{14}C and ^{10}Be data indicate that the summit of Mt. Washington began to be exposed early in the last deglaciation and at least several kyr before the withdrawal of ice from the lowlands – a critical constraint on the thinning of the southeast sector of the LIS. Taken at face value, estimates of summit deglaciation based on the central tendency of relevant ^{10}Be and in-situ ^{14}C measurements disagree by several thousand years; however, this apparent discrepancy may not be real. Cosmogenic exposure ages are by their nature uncertain for concentrations near saturation. In this case, ^{14}C ages for summit samples are consistent with 18 ka exposure at the 2σ level, considering both analytical and production rate uncertainties (Fig. 4). It is also possible that laboratory procedures have caused us to overestimate ^{14}C content in these samples. Froth flotation solution, which we used for mineral separation, can introduce ^{14}C contamination (Nichols and Goehring, 2019), which may have elevated ^{14}C concentrations in our samples. This latter point could explain why the summit ^{14}C age of 17.9 ± 3.5 ka, from Bierman et al. (2015) and for which froth flotation was not used, is younger than the ^{14}C ages we measured and agrees

closely with the ^{10}Be-inferred timing of deglaciation. However, lower elevation samples where no ^{10}Be-in-situ ^{14}C disagreement exists (Fig 5B) generally rules out this possibility since all samples underwent the same froth-flotation procedure.

There are also reasonable geologic scenarios consistent with discrepancies between ^{10}Be and in-situ ^{14}C exposure ages. Modeling shows that ^{14}C concentrations similar to those of the summit samples could be reached with 18 kyr of postglacial exposure if surfaces had been long-exposed (>10 kyr) prior to the LGM and experienced minimal burial by ice (<4 kyr) and erosion (<30 cm) under brief, cold-based LGM ice cover (Fig. 7). The apparently older in-situ ^{14}C ages in this case would reflect inheritance of ^{14}C from pre-LGM exposure since the last interglacial (Fig. 8) and limit the onset of summit ice cover to after 22 ka (Fig. 7), in line with the late LIS advance into New England from other dating constraints.

The Flanks of Mount Washington: Efficient Erosion and Rapid Ice Sheet Retreat during the Bølling Warm Period

Unlike the wide-ranging and largely inherited ^{10}Be concentrations from the alpine lawns and summit cone, the ^{10}Be ages below 1600 m a.s.l. closely agree with each other and with the ~14 ka timing of deglaciation in the lowlands inferred from other methods (Ridge et al., 2012; Thompson et al., 2017; Bromley et al., 2015, 2019). These ^{10}Be ages are concordant with two in-situ ^{14}C ages at 1370 m a.s.l. (MW-15, 11.3 ± 1.8 ka; MW-13, 15.6 ± 3.5 ka). It appears that surfaces lower on the mountain were eroded during the last glaciation, effectively removing most nuclides from pre-LGM exposure. We thus interpret the ^{10}Be ages below 1600 m a.s.l. to record the timing of deglaciation.

The similarity of the ^{10}Be ages between 1600 and 700 m a.s.l. suggests rapid deglaciation between 15 and 13 ka (14.1 ± 0.9 ka [mean, 1SD, n=9], or ± 1.1 ka including the 4.9% ^{10}Be production rate uncertainty [Balco et al., 2009]). Nearby deglacial chronological constraints help place limits on the timing of ice withdrawal from even lower elevations in the region (~200–400 m a.s.l.) (Fig. 1). Connecticut River valley varves ~50 km to the west suggest that the LIS margin retreated to a latitude north of Mount Washington at ~14.2 ka (Ridge et al., 2012), while ^{10}Be ages from the Littleton-

Bethlehem and Berlin moraines record subsequent LIS readvances just north of the Presidential Range at 13.8 ± 0.2 ka (n=4) and 13.7 ± 0.6 ka (n=7) (Balco et al., 2009; Thompson et al., 2017; Bromley et al., 2019). Taken together, these data suggest that the LIS surface lowered >1000 m in the Mount Washington area at ~14 ka within approximately a thousand years, and perhaps over substantially less time.

Simple modeling supports our interpretation of early deglaciation at high elevations on Mount Washington and rapid LIS thinning down the rest of the mountain at ~14 ka. Assuming a perfectly plastic ice rheology and a basal shear stress of 50 kPa, we calculated theoretical ice-sheet profiles from the coast of Connecticut to Mount Washington (Benn and Evans, 2010) (Supplemental Table S4). By simulating the retreat of the ice sheet margin as constrained by dated varves up the Connecticut River valley (Ridge et al., 2012), the profiles suggest the times at which different elevations became ice free on Mount Washington (Fig. 9A). This simple model predicts thin summit ice cover at the LGM and gradual thinning down the top few hundred meters of the mountain after initial exposure at ~19 ka, followed by rapid ice-surface lowering at ~14.5 ka, in good agreement with our dataset (Fig. 9B). Assuming higher or lower basal shear stresses would change the calculated ice thicknesses at Mount Washington by up to several hundred meters–and thus if or when the summit was ice covered–but the general pattern of gradual initial ice surface lowering transitioning to rapid deglaciation at ~14.5 ka is robust.

Ice thickness and margin records elsewhere in the region suggest that the abrupt withdrawal of ice from Mount Washington reflects rapid retreat of the LIS through the interior of the northeastern United States, likely during Bølling warming (Fig. 10A). Vertical transects of cosmogenic nuclide ages at Mount Mansfield, Vermont (Corbett et al., 2019) and in the Adirondack Mountains, New York (Barth et al., 2019) parallel the results from Mount Washington, recording rapid ice-surface lowering at 13.9 ± 0.6 ka in Vermont and in between 15.4 ± 1.0 ka and 13.9 ± 0.9 ka in New York (Fig. 10C). Meanwhile, varve records in the Connecticut River valley and in Hudson/Champlain valley suggest that northward LIS retreat across the region accelerated several-fold at the onset of the Bølling at 14.6 ka (Fig. 10B). Varves thickened due to greater sediment delivery to proglacial lakes, implying increased summer ice melt (Ridge et al., 2012).

CONCLUSIONS

Twenty new and five previously published (Bierman et al., 2015) ^{10}Be measurements from Mount Washington, New Hampshire show an increasing age trend with elevation above 1600 m a.s.l., reaching ages >100 ka on the summit. These old ages suggest that the upper reaches of the mountain were covered by weakly erosive, at least in part cold-based ice during the last glaciation, allowing nuclides produced before the LGM to persist in bedrock and boulder surfaces. The youngest ^{10}Be and in-situ ^{14}C ages from the uplands suggest that the high elevations deglaciated by 18 ka, whether from the disappearance of a local ice cap or early LIS thinning. Summit erratics would be useful to date to determine if the LIS overtopped the Presidential Range during the most recent glacial cycle, as has been done in Baffin Island and Scotland (Marsella et al., 2000; Fabel et al., 2012). Younger and indistinguishable ^{10}Be and in-situ ^{14}C ages below 1600 m a.s.l. imply deeper erosion there during the last glaciation, presumably by warm-based ice, and suggest rapid ice-sheet thinning at 14.1 ± 1.1 ka. Abrupt ice-surface lowering and margin retreat documented elsewhere in interior northeastern U.S.A. suggests that there may have been considerable ice-volume loss across the region at this time, coincident with the Northern Hemisphere Bølling warm period.

ACKNOWLEDGMENTS

This research was funded by NSF-EAR 1603175 to J. Shakun, NSF-EAR 1602280 and NSF-EAR 1735676 to P. Bierman, and NSF-EAR 1603224 to P. T. Davis. We thank B. Higginbotham for help with sample collection in the field and A. Denn with sample processing. NOSAMS performed AMS ^{14}C measurements. We thank Woodrow Thompson, John Stone, and two other anonymous reviewers who helped improve this manuscript. John Stone, in particular, provided us with many challenging questions, including some that we could not fully answer based on our data. This is Lawrence Livermore National Laboratory contribution LLNL-JRNL-769071.

REFERENCES CITED

Anderson, R.S., Davis, R.B., Miller, N.G., and Stuckenrath, R., 1986, History of late- and post-glacial vegetation and disturbance around Upper South Branch Pond, northern Maine: Canadian Journal of Botany, v. 64, p. 1977–1986, doi: 10.1139/b86-262.

Antevs, E., 1932, Alpine Zone of Mount Washington Range: Auburn, Maine, Merrill and Webber Co., 118 p.

Balco, G., and Schaefer, J.M., 2006, Cosmogenic-nuclide and varve chronologies for the deglaciation of southern New England: Quaternary Geochronology, v. 1, p. 15–28, doi:10.1016/j.quageo.2006.06.014

Balco, G., Stone, J.O., Porter, S.C., and Caffee, M.W., 2002, Cosmogenic-nuclide ages for New England coastal moraines, Martha's Vineyard and Cape Cod, Massachusetts, USA: Quaternary Science Reviews, v. 21, p. 2127–2135, doi:10.1016/S0277-3791(02)00085-9

Balco, G., Stone, J.O., Lifton, N.A., and Dunai, T.J., 2008, A complete and easily accessible means of calculating surface exposure ages or erosion rates from ^{10}Be and ^{26}Al measurements: Quaternary Geochronology, v. 3, p. 174–195, doi:10.1016/j.quageo.2007.12.001.

Balco, G., Briner, J., Finkel, R.C., Rayburn, J.A., Ridge, J.C., and Schaefer, J.M., 2009, Regional beryllium-10 production rate calibration for late-glacial northeastern North America: Quaternary Geochronology, v. 4, p. 93–107, doi:10.1016/j.quageo.2008.09.001

Ballantyne, C.K. and Stone, J.O., 2015, Trimlines, blockfields and the vertical extent of the last ice sheet in Southern Ireland: Boreas, v. 44, p. 277–287, doi:10.1111/bor.12109

Barth, A.M., Marcott, S.A., Licciardi, J.M., and Shakun, J.D., 2019, Deglacial thinning of the Laurentide Ice Sheet in the Adirondack Mountains, New York, USA, revealed by ^{36}Cl

exposure dating: Paleoceanography and Paleoclimatology, v. 34, p. 946–953, doi:10.1029/2018PA003477

Batchelor, C.L., Margold, M., Krapp, M., Murton, D.K., Dalton, A.S., Stokes, C.R., Murton, J.B., Manica, A., and Gibbard, L., 2019, The configuration of Northern Hemisphere ice sheets through the Quaternary: Nature Communications, p. 1–10, doi:10.1038/s41467-019-11601-2.

Benn, D.I., and Evans, D.J.A., 2010, Glaciers and glaciation: New York, Toutledge, 802 p.

Bierman, P.R., Davis, P.T., Corbett, L.B., Lifton, N.A., and Finkel, R.C., 2015, Cold-based Laurentide ice covered New England's highest summits during the Last glacial maximum: Geology, v. 43, p. 1059–1062, doi:10.1130/G37225.1

Borchers, B., Marrero, S., Balco, G., Caffee, M., Goehring, B., Lifton, N., Nishiizumi, K., Phillips, F., Schaefer, J., and Stone, J., 2016, Geological calibration of spallation production rates in the CRONUS-Earth project: Quaternary Geochronology, v. 31, p. 188–198, doi:10.1016/j.quageo.2015.01.009

Briner, J.P., Miller, G.H., Davis, P.T., and Finkel, R.C., 2006, Cosmogenic radionuclides from fiord landscapes support differential erosion by overriding ice sheets: Geological Society of American Bulletin, v. 118, p. 406–420, doi:10.1130/B25716.1.

Bromley, G.R.M., Hall, B.L., Thompson, W.B., Kaplan, M.R., Garcia, J.L., and Schaefer, J.M., 2015, Late glacial fluctuations of the Laurentide Ice Sheet in the White Mountains of Maine and New Hampshire, U.S.A.: Quaternary Research, v. 83, p. 522–530, doi:10.1016/j.yqres.2015.02.004

Bromley, G.R.M., Hall, B.L., Thompson, W.B., and Lowell, T.V., 2019, Age of the Berlin moraine complex, New Hampshire, USA, and implications for ice sheet dynamics and climate during Termination 1: Quaternary Research, p. 1–14, doi: 10.1017/qua.2019.66.

Brook, E.J., Nesje, A., Lehman, S.J., Raisbeck, G.M., and Yiou, F., 1996, Cosmogenic nuclide exposure ages along a vertical transect in western Norway: Implications for the height of the Fennoscandian ice sheet: Geology, v. 24, p. 207–210, doi:10.1130/0091-7613(1996)024<0207:CNEAAA>2.3.CO;2

Carlson, A.E., Tarasov, L., and Pico, T., 2018, Rapid Laurentide ice-sheet advance towards southern last glacial maximum limit during marine isotope stage 3: Quaternary Science Reviews, v. 196, p. 118–123, doi:10.1016/j.quascirev.2018.07.039

Chmeleff, J., von Blanckenburg, F., Kossert, K., and Jakob, D., 2010, Determination of the ^{10}Be half-life by multicollector ICP-MS and liquid scintillation counting: Nuclear Instruments and Methods in Physics Research, B, v. 268, p. 192–199, doi:10.1016/j.nimb.2009.09.012

Clark, G.M., and Schmidlin, T.W., 1992, Alpine periglacial landforms of eastern North America: A review: Permafrost and Periglacial Processes, v. 3, p. 225–230, https://doi.org/10.1002/ppp.3430030309

Clark, P.U. et al., 1993, Initiation and development of the Laurentide and Cordilleran Ice Sheets following the last interglaciation: Quaternary Science Reviews, v. 12, p. 79–114, doi:10.1016/0277-3791(93)90011-A.

Corbett, L.B., Bierman, P.R., Graly, J.A., Neumann, T.A., and Rood, D.H., 2013, Constraining landscape history and glacial erosivity using paired cosmogenic nuclides in Upernavik,

northwest Greenland: Bulletin of the Geological Society of America, v. 125, p. 1539–1553, doi:10.1130/B30813.1

Corbett, L.B., Bierman, P.R., and Rood, D.H., 2016, An approach for optimizing in-situ cosmogenic ^{10}Be sample preparation: Quaternary Geochronology, v. 33, p. 24–34, doi:10.1016/j.quageo.2016.02.001

Corbett, L.B., Bierman, P.R., Stone, B.D., and Caffee, M.W., 2017, Cosmogenic nuclide age estimates for Laurentide Ice Sheet recession from the terminal moraine, New Jersey, USA, and constraints on Latest Pleistocene ice sheet behavior: Quaternary Research, v. 87, p. 482–498, doi.org/10.1017/qua.2017.11

Corbett, L.B., Bierman, P.R., Wright, S.F., Shakun, J.D., Davis, P.T., Goehring, B.M., Halsted, C.T., Koester, A.J., Caffee, M.W., and Zimmerman, S.R., 2019, Analysis of multiple cosmogenic nuclides constrains Laurentide Ice Sheet history and process on Mt. Mansfield, Vermont's highest peak: Quaternary Science Reviews, v. 205, p. 234–246, doi:10.1016/j.quascirev.2018.12.014

Cwynar, L.C., and Spear, R.W., 2001, Lateglacial climate change in the White Mountains, New Hampshire: Quaternary Science Reviews, v. 20(11), p. 1265–1274, https://doi.org/10.1016/S0277-3791(00)00151-7

Davis, P.T., 1988, Holocene glacier fluctuations in the American Cordillera: Quaternary Science Reviews, v. 7(2), p. 129–157, https://doi.org/10.1016/0277-3791(88)90003-0

Davis, P.T., 1999, Cirques of the Presidential Range, New Hampshire, and surrounding alpine areas in the northeastern United States: Géographie Physique et Quaternaire, v. 53, p. 25–44, https://doi.org/10.7202/004784ar

Davis, P.T., and Davis, R.B., 1980, Interpretation of minimum-limiting radiocarbon dates for deglaciation of Mount Katahdin area, Maine: Geology, v. 8, p. 396–400, https://doi.org/10.1130/0091-7613(1980)8<396:IOMRDF>2.0.CO;2

Davis, P.T., Bierman, P.R., Corbett, L.B., and Finkel, R.C., 2015, Cosmogenic exposure age evidence for rapid Laurentide deglaciation of the Katahdin area, west-central Maine, USA, 16 to 15 ka: Quaternary Science Reviews, v. 116, p. 95–105, doi:10.1016/j.quascirev.2015.03.021

Davis, P.T., Shakun, J.D., Bierman, P.R., Koester, A.J., and Corbett, L.B., 2017, Testing the cosmogenic nuclide dipstick model for deglaciation of Mount Washington. *in* Eusden, J.D. and Retelle, M. (eds.), Guidebook for Field Trips in Northwestern Maine and Northern New Hampshire, New England Intercollegiate Geological Conference, 109th annual meeting, Bethel, Maine, p. 247-272 https://doi.org/10.26780/2017.001.0014

Dredge, L. and Thorleifson, L., 1987, The middle Wisconsinan history of the Laurentide Ice Sheet: Géographie physique et Quaternaire, v. 41(2), p. 215–235, https://doi.org/10.7202/032680ar

Dyke, A.S., Moore, A., and Robertson, L., 2003, Deglaciation of North America. Geological Survey of Canada Open File, 1574. Thirty-two digital maps at 1:7,000,000 scale with accompanying digital chronological database and one poster (two sheets) with full map series.

Dyke, A.S., 2004, An outline of the deglaciation of North America with emphasis on central and northern Canada: Quaternary Glaciations-Extent and Chronology, Part II: North America, v. 2b, p. 373–424, doi:10.1016/S1571-0866(04)80209-4

Eusden, J.D., and Fowler, B.K., 2013, Uplift and erosion of the White Mountains, *in* Eusden, J.D., Thompson, W.B., Fowler, B.K., Davis, P.T., Bothner, W.A., Boisvert, R.A., and Creasy, J., The Geology of New Hampshire's White Mountains. Durand Press, Lyme, NH, p. 87-96.

Fabel, D., Ballantyne, C.K., and Xu, S., 2012, Trimlines, blockfields, mountain-top erratics and the vertical dimensions of the last British-Irish Ice Sheet in NW Scotland: Quaternary Science Reviews, v. 55, p. 91–102. doi:10.1016/j.quascirev.2012.09.002

Fernald, M.L., 1925, Persistence of plants in unglaciated areas of boreal America: Memoirs of the American Academy of Arts and Sciences, v. 15, p. 237-342.

Flint, R.F., 1951, Highland centers of former glacier outflow in northeastern North America: Geological Society of America Bulletin, v. 62, p. 21–38, https://doi.org/10.1130/0016-7606(1951)62[21:HCOFGO]2.0.CO;2

Fowler, B.K., Thompson, W.B., and Davis, P.T., 2013, Glaciers shape the mountains, *in* Eusden, J.D., Thompson, W.B., Fowler, B.K., Davis, P.T., Bothner, W.A., Boisvert, R.A., and Creasy, J., The Geology of New Hampshire's White Mountains. Durand Press, Lyme, NH, p. 97–108.

Gjermundsen, E.F., Briner, J.P., Akçar, N., Foros, J., Kubik, P.W., Salvigsen, O. and Hormes, A., 2015, Minimal erosion of Arctic alpine topography during late Quaternary glaciation: Nature Geoscience, v. 8, p. 789–792, https://doi.org/10.1038/ngeo2524

Goehring, B.M., Brook, E.J., Linge, H., Raisbeck, G.M., and Yiou, F., 2008, Beryllium-10 exposure ages of erratic boulders in southern Norway and implications for the history of the Fennoscandian Ice Sheet: Quaternary Science Reviews, v. 27, p. 320–336, doi:10.1016/j.quascirev.2007.11.004

Goehring, B.M., Balco, G., Todd, C., Moening-Swanson, I., Nichols, K., and Sites, F., 2019a, Late-glacial grounding line retreat in the northern Ross Sea, Antarctica: Geology v. 47, p. 1–4, doi:10.1130/G45413.1/4648018/g45413.pdf

Goehring, B.M., Wilson, J., and Nichols, K., 2019b, A fully automated system for the extraction of in-situ cosmogenic carbon-14 in the Tulane University cosmogenic nuclide laboratory: Nuclear Instruments & Methods in Physics Research Section B-Beam Interactions with Materials and Atoms, v 455, p. 284–292, doi.org/10.1016/j.nimb.2019.02.006

Goldthwait, J.W., 1913, Glacial cirques near Mount Washington: American Journal of Science, v. 35, p. 1–19.

Goldthwait, J.W., 1916, Glaciation in the White Mountains of New Hampshire: Bulletin of the Geological Society of America, v. 27, p. 263–294, doi:10.1130/GSAB-27-263

Goldthwait, R.P., 1940, Geology of the Presidential Range. New Hampshire Academy of Science Bulletin, v. 1, p. 43

Goldthwait, R.P., 1970a, Fieldguide for Friends of the Pleistocene, 33rd Annual Reunion, *in* Goldthwait, R.P., cd., Scientific aspects of Mount Washington in New Hampshire, Columbus, The Ohio State University, 31 p.

Goldthwait, R.P., 1970b, Mountain glaciers of the Presidential Range in New Hampshire: Arctic and Alpine Research, v. 2, p. 85–102, doi:10.1657/1523-0430(07-069)

Goldthwait, R.P., Billings, M.P., and Creasy, J.W., 1987, Mount Washington-Crawford Notch area, New Hampshire, *in* Roy, D.C., cd., North-Eastern Section of the Geological Society of American Centennial Field Guide, p. 257–262

Gosse, J.C. and Phillips, F.M., 2001, Terrestrial in-situ cosmogenic nuclides: theory and application: Quaternary Science Reviews, v. 20, p. 1475–1560, doi:10.1016/S0277-3791(00)00171-2

Hall, B.L., Borns, H.W., Bromley, G.R.M., and Lowell, T.V., 2017, Age of the Pineo Ridge system: Implications for behavior of the Laurentide Ice Sheet in eastern Maine, U.S.A., during the last deglaciation: Quaternary Science Reviews, v. 169, p. 344–356, doi:10.1016/j.quascirev.2017.06.011

Jull, A.J.T., Scott, E.M., and Bierman, P., 2015, The CRONUS-Earth inter-comparison for cosmogenic isotope analysis: Quaternary Geochronology, v. 26, p. 3–10, doi:10.1016/j.quageo.2013.09.003

Koester, A.J., Shakun, J.D., Bierman, P.R., Davis, P.T., Corbett, L.B., Braun, D., and Zimmerman, S.R., 2017, Rapid thinning of the Laurentide Ice Sheet in coastal Maine, USA, during late Heinrich Stadial 1: Quaternary Science Reviews, v. 163, p. 1–13, http://dx.doi.org/10.1016/j.quascirev.2017.03.005

Kohl, C.P., and Nishiizumi, K., 1992, Chemical isolation of quartz for measurement of in-situ-produced cosmogenic nuclides: Geochimica et Cosmochimica Acta, v. 56, p. 3583–3587, doi:10.1016/0016-7037(92)90401-4

Korschinek, G., Bergmaier, A., Faestermann, T., Gerstmann, U.C., Knie, K., Rugel, G., Wallner, A., Dillmann, I., Dollinger, G., Lierse von Gostomski, C., Kossert, K., Maiti, M., Poutivtsev, M., and Remmert, A., 2010, A new value for the half-life of ^{10}Be by Heavy-Ion Elastic Recoil Detection and liquid scintillation counting: Nuclear Instruments and Methods in Physical Research B, v. 268, p. 187–191, doi:10.1016/j.nimb.2009.09.020

Lal, D., 1991, Cosmic ray labeling of erosion surfaces: in situ nuclide production rates and erosion models: Earth and Planetary Science Letters, v. 104, p. 424–439, doi:10.1016/0012-821X(91)90220-C.

Lambeck, K., Rouby, H., Purcell, A., Sun, Y., and Sambridge, M., 2014, Sea level and global ice volumes from the Last Glacial Maximum to the Holocene: Proceedings of the National Academy of Sciences, v. 111, p. 15296–15303, doi:10.1073/pnas.1411762111

Lifton, N., Sato, T., and Dunai, T.J., 2014, Scaling in-situ cosmogenic nuclide production rates using analytical approximations to atmospheric cosmic-ray fluxes: Earth and Planetary Science Letters, v. 386, p. 149–160, https://doi.org/10.1016/j.epsl.2013.10.052

Lifton, N.A., Phillips, F.M., and Cerling, T.E., 2016, Using Lake Bonneville features to calibrate in-situ cosmogenic nuclide production rates, 1st ed, Developments in earth surface processes. Elsevier B.V. doi:10.1016/B978-0-444-63590-7.00009-3

Marquette, G.C., Gray, J.T., Gosse, J.C., Courchesne, F., Stockli, L., Macpherson, G., and Finkel, R., 2004, Felsenmeer persistence under non-erosive ice in the Torngat and Kaumajet Mountains, Quebec and Labrador, as determined by soil weathering and cosmogenic nuclide exposure dating: Canadian Journal of Earth Sciences, v. 41, p. 19–38, doi:10.1139/E03-072

Marsella, K.A., Bierman, P.R., Davis, P.T., and Caffee, M.W., 2000, Cosmogenic ^{10}Be and ^{26}Al ages of the Last Glacial Maximum, Eastern Baffin Island, Arctic Canada: Bulletin of the Geologic Society of America, v. 112, p. 1296–1312, doi: 10.1130/0016-7606(2000)112<1296:CBAAAF>2.0.CO;2

Munroe, J.S., Perzan, Z.M., and Amidon, W.H., 2016, Cave sediments constrain the latest Pleistocene advance of the Laurentide Ice Sheet in the Champlain Valley, Vermont, USA.;Journal of Quaternary Science, v. 31, p. 893–904. doi:10.1002/jqs.2913

Nichols, K.A., and Goehring, B.M., 2019, Isolation of quartz for cosmogenic in situ ^{14}C analysis: Geochronology Discussions, p. 1–14. doi:https://doi.org/10.5194/gchron-2019-7

Nishiizumi, K., Imamura, M., Caffee, M.W., Southon, J.R., Finkel, R.C., and McAninch, J., 2007, Absolute calibration of ^{10}Be AMS standards: Nuclear Instruments and Methods in Physics Research Section B: Beam Interactions with Materials and Atoms, v. 258, p. 403–413, doi:10.1016/j.nimb.2007.01.297

North Greenland Ice Core Project members, 2004, High-resolution record of Northern Hemisphere climate extending into the last interglacial period: Nature, v. 431, p. 147–151, https://doi.org/10.1038/nature02805.

Parent, M. and Dubé-Loubert, 2017, Middle and Late Wisconsinan events and stratigraphy in southern Québec – A new pre-LGM marine incursion. Northeast Friends of the Pleistocene field trip guidebook, 80th annual meeting, Mont St. Hilaire, Québec, 29 pp.

Peteet, D.M., Beh, M., Orr, C., Kurdyla, D., Nichols, J., and Guilderson, T., 2012, Delayed deglaciation or extreme Arctic conditions 21–16 cal. Kyr at southeastern Laurentide Ice Sheet margin?: Geophysical Research Letters, v. 39, L11706, doi:10.1029/2012GL051884.

Pewe, T.L., 1983, Alpine permafrost in the contiguous United States: A review. Arctic and Alpine Research 15(2), 145–156. doi:10.1080/00040851.1983.12004339

Pico, T., Creveling, J.R., and Mitrovica, J.X., 2017, Sea-level records from the U.S. mid-Atlantic constrain Laurentide Ice Sheet extent during Marine Isotope Stage 3: Nature Communications, v. 8, p. 1–6, doi:10.1038/ncomms15612

Pico, T., Mitrovica, J.X., Braun, J., and Ferrier, K.L., 2018, Glacial isostatic adjustment deflects path of the ancestral Hudson River: Geology, v. 46, p. 1–4. doi:10.1130/G40221.1

Reimer, P., Bard, E., Bayliss, A., Beck, J.W., Blackwell, P.G., Ramsey, C.B., Buck, C.E., Cheng, H., Edwards, R.L., Friedrich, M., Grootes, P.M., Guilderson, T.P., Haflidason, H., Hajdas, I., Hatee, C., Heaton, J., Hoffmann, D.L., Hogg, A.G., Hughen, K.A., F., K.K., Kromer, B., Manning, S.W., Niu, M., Reimer, R.W., Richards, D.A., Scott, E.M., Southon, J.R., Staff, R.A., Turney, C.S.M., and van der Plicht, J., 2013, IntCal13 and Marine13 Radiocarbon Age Calibration Curves 0–50,000 Years cal BP: Radiocarbon, v. 55, p. 1869–1887, doi:10.2458/azu_js_rc.55.16947

Ridge, J.C., Balco, G., Bayless, R.L., Beck, C.C., Carter, L.B., Dean, J.L., Voytek, E.B., and Wei, J.H., 2012, The new North American Varve Chronology: A precise record of southeastern Laurentide Ice Sheet deglaciation and climate, 18.2–12.5 kyr BP, and correlations with Greenland ice core records: American Journal of Science, v. 312, p. 685–722, doi:10.2475/07.2012.01

Rogers, J.N., 2003, Major Holocene debris flows of Franconia Notch (White Mountains, New Hampshire) recorded in Profile Lake. [M.S. thesis]: Amherst, University of Massachusetts, 182 p.

Spear, R.W., 1989, Late Quaternary history of high-elevation vegetation in the White Mountains of New Hampshire: Ecological Monographs, v. 59(2), p. 125–151, https://doi.org/10.2307/2937283

Spear, R.W., Davis, M.B. and Shane, L.C., 1994, Late Quaternary history of low-and mid-elevation vegetation in the White Mountains of New Hampshire: Ecological Monographs, v. 64(1), p. 85–109, https://doi.org/10.2307/2937056

Stone, J.O., 2000, Air pressure and cosmogenic isotope production: Journal of Geophysical Research, v. 105, p. 753–759, doi:10.1029/2000JB900181.

Stuiver, M., Reimer, P.J., and Reimer, R.W., 2015, CALIB 7.1 [WWW program] at: http://calib.org

Thompson, W.B., Dorion, C.C., Ridge, J.C., Balco, G., Fowler, B.K., and Svendsen, K.M., 2017, Deglaciation and late-glacial climate change in the White Mountains, New Hampshire, USA: Quaternary Research, v. 87, p. 96–120, doi:10.1017/qua.2016.4

Thompson, W.F., 1960, The shape of New England mountains. Part I. Appalachia, v. 26, p. 145–159.

Thompson, W.F., 1961a, The shape of New England mountains, Part II. Appalachia, v. 27, p. 316–335.

Thompson, W.F., 1961b, The shape of New England mountains, Part III. Appalachia, v. 27, p. 457–478.

Winsor, K., Carlson, A.E., Caffee, M.W., and Rood, D.H., 2015, Rapid last-deglacial thinning and retreat of the marine-terminating southwestern Greenland ice sheet: Earth and Planetary Science Letters, v. 426, p. 1–12, doi:10.1016/j.epsl.2015.05.040

FIGURE CAPTIONS

Figure 1: Laurentide Ice Sheet deglaciation ages in New England. Isochrons from North American Varve Chronology of deglaciation (from Fig. 12 in Ridge et al. (2012)). Black dots are moraines and black triangles are mountain summits and slopes dated with ^{10}Be; ages calculated using the northeastern North American production rate (Balco et al., 2009) and LSDn scaling (Lifton et al., 2014). The heavy black line is the maximum extent of the LIS (Dyke, 2003).

Figure 2: Representative samples from Mount Washington with ^{10}Be and in-situ ^{14}C ages showing external uncertainty. **(A)** Frost-riven block on the summit (1907 m a.s.l.). **(B)** Large boulder ~50 m elevation below the summit (1851 m a.s.l.). **(C)** Rôche moutonnée on Bigelow Lawn with patterned ground in foreground and the summit in the background (1665 m a.s.l.). **(D)** Large boulder on Bigelow Lawn with the summit in the background (1614 m a.s.l.). **(E)** Bedrock surface on Square Ledge in Pinkham Notch (730 m a.s.l.). **(F)** Sub-rounded boulder halfway down the mountain (1370 m a.s.l.). **(G)** Aerial oblique view looking west towards Mount Washington with Pinkham Notch in the foreground showing sample locations. (Google Earth, 2018)

Figure 3: A LiDAR digital elevation model of Mount Washington showing ^{10}Be and in-situ ^{14}C ages with 1σ external uncertainties (in ka) generated in this study (black outlined boxes). Ages are ^{10}Be unless denoted by "(^{14}C)". Bierman et al. (2015) sample ages shown in gray. Bedrock samples are squares, frost-riven blocks are triangles, and boulder samples are circles. Ages grouped together with brackets from closely-spaced samples. Inset map shows location of Mount Washington in northern New Hampshire.

Figure 4: Mount Washington in-situ ^{14}C concentrations with 1σ analytical uncertainties (5.6%) plotted against elevation. Dashed lines are exposure isochrons in 2 kyr intervals from 2 ka to 24

ka. Gray shading represents saturation with 1σ production rate uncertainty (5.6%; Goehring et al., 2019). Isochrons calculated using same production rate and scaling scheme as sample ages reported in text. Sample PTMW03 from Bierman et al. (2015) shown with its published uncertainty in gray.

Figure 5: (A) ^{10}Be (solid) and in-situ ^{14}C (hollow) ages of boulders (circles), bedrock (squares), and frost-riven blocks (triangles) from Mount Washington with 1σ external uncertainties (smaller than symbol size for many samples). Samples with saturated ^{14}C concentrations designated by arrows at their respective elevation. Ages from Bierman et al. (2015) are shown in gray. **(B)** Zoom in of data in panel A from 25 to 5 ka.

Figure 6: ^{14}C/^{10}Be ratios versus ^{10}Be concentrations of samples for which both nuclides measured in this study, as well as summit sample PTMW-03 from Bierman et al. (2015). Nuclide concentrations normalized by the local production rate at each sample location (i.e., concentrations scaled to production rate of 1 atom g^{-1} yr^{-1}). All samples plot near the continuous exposure line, suggesting that they experienced minimal or no burial.

Figure 7: Glaciation histories consistent with summit ^{14}C concentrations, assuming deglaciation at 18 ka. Contours show the glaciation age that would yield the average ^{14}C concentration of the three summit samples (MW-22, MW-23, PTMW-03) for a given combination of pre-LGM exposure duration (y-axis) and LGM erosion depth (x-axis). Solid isochrons are plausible solutions, whereas dashed isochrons place the onset of ice cover after deglaciation and are therefore implausible.

Figure 8: Modeled ^{10}Be (top) and in-situ ^{14}C (bottom) concentrations for the samples from >1600 m a.s.l. in which both nuclides measured in this study, assuming continuous exposure since the last interglacial at 130 ka, except for brief LGM ice cover from 20 to 18 ka. Error bars

on left show measured sample concentrations with 1σ analytical uncertainties. Erosion depths during LGM ice cover adjusted to produce ^{10}Be concentrations consistent with measured values. Nuclide concentrations normalized by local production rate at each sample location (i.e., concentrations scaled to production rate of 1 atom g^{-1} yr^{-1}).

Figure 9: (A) Ice sheet profiles projected from LIS margin up Connecticut River valley to Mount Washington assuming a basal shear stress of 50 kPa (Benn and Evans, 2010; Supplemental Table S4). Each line represents a time step in North American Varve Chronology (Ridge et al., 2012). **(B)** Projected ice-sheet surface elevations at Mount Washington (blue dots) compared to our exposure data from Figure 5.

Figure 10: (A) NGRIP Greenland ice core δ^{18}O record (North Greenland Ice Core Project members, 2004), a proxy for North Atlantic temperature. **(B)** LIS margin retreat in central New England based on North American Varve Chronology (after Ridge et al., 2012) **(C)** In-situ ^{14}C and ^{10}Be ages from Mount Washington, New Hampshire (this study, black; Bierman et al. (2015), gray), Mount Mansfield, Vermont (brown) (Corbett et al., 2019), and ^{36}Cl ages from the Adirondack Mountains (green) (Barth et al., 2019) showing 1σ external uncertainties. Pale blue bar highlights Bølling/Allerød interval.

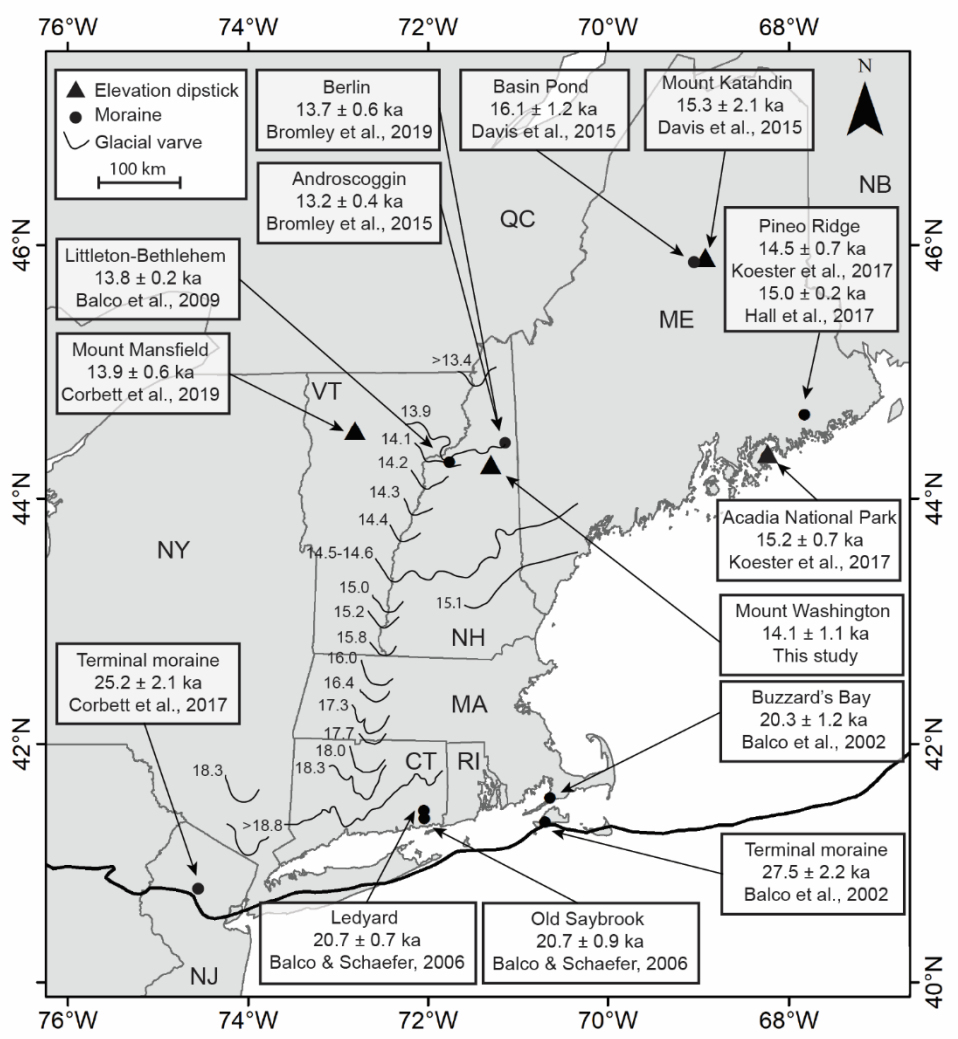
76°W
74°W
72°W
70°W
68°W
46°N
44°N
42°N
40°N
N
Elevation dipstick
Moraine
Glacial varve
100 km
Berlin
13.7 ± 0.6 ka
Bromley et al., 2019
Basin Pond
16.1 ± 1.2 ka
Davis et al., 2015
Mount Katahdin
15.3 ± 2.1 ka
Davis et al., 2015
Androscoggin
13.2 ± 0.4 ka
Bromley et al., 2015
Littleton-Bethlehem
13.8 ± 0.2 ka
Balco et al., 2009
Pineo Ridge
14.5 ± 0.7 ka
Koester et al., 2017
15.0 ± 0.2 ka
Hall et al., 2017
Mount Mansfield
13.9 ± 0.6 ka
Corbett et al., 2019
Acadia National Park
15.2 ± 0.7 ka
Koester et al., 2017
Mount Washington
14.1 ± 1.1 ka
This study
Terminal moraine
25.2 ± 2.1 ka
Corbett et al., 2017
Buzzard's Bay
20.3 ± 1.2 ka
Balco et al., 2002
Terminal moraine
27.5 ± 2.2 ka
Balco et al., 2002
Ledyard
20.7 ± 0.7 ka
Balco & Schaefer, 2006
Old Saybrook
20.7 ± 0.9 ka
Balco & Schaefer, 2006
NB
QC
ME
VT
NY
NH
MA
CT
RI
NJ
>13.4
13.9
14.1
14.2
14.3
14.4
14.5-14.6
15.0
15.1
15.2
15.8
16.0
16.4
17.3
17.7
18.0
18.3
18.3
>18.8

Figure 1

720

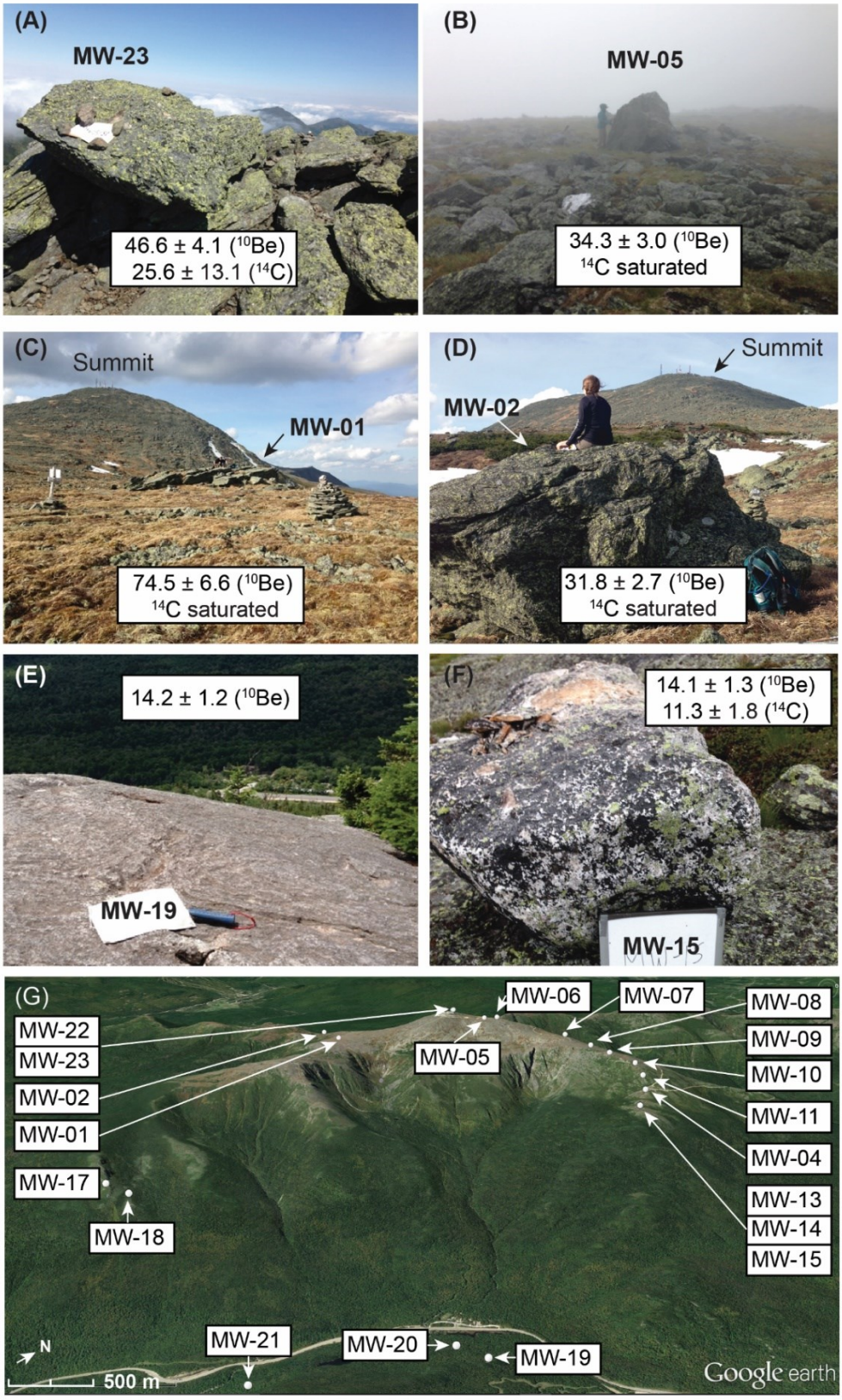
(A)
MW-23
46.6 ± 4.1 (10Be)
25.6 ± 13.1 (14C)
(B)
MW-05
34.3 ± 3.0 (10Be)
14C saturated
(C)
Summit
MW-01
74.5 ± 6.6 (10Be)
14C saturated
(D)
Summit
MW-02
31.8 ± 2.7 (10Be)
14C saturated
(E)
14.2 ± 1.2 (10Be)
MW-19
(F)
14.1 ± 1.3 (10Be)
11.3 ± 1.8 (14C)
MW-15
(G)
MW-22
MW-23
MW-02
MW-01
MW-17
MW-18
MW-06
MW-07
MW-05
MW-08
MW-09
MW-10
MW-11
MW-04
MW-13
MW-14
MW-15
MW-21
MW-20
MW-19
N
500 m
Google earth

Figure 2

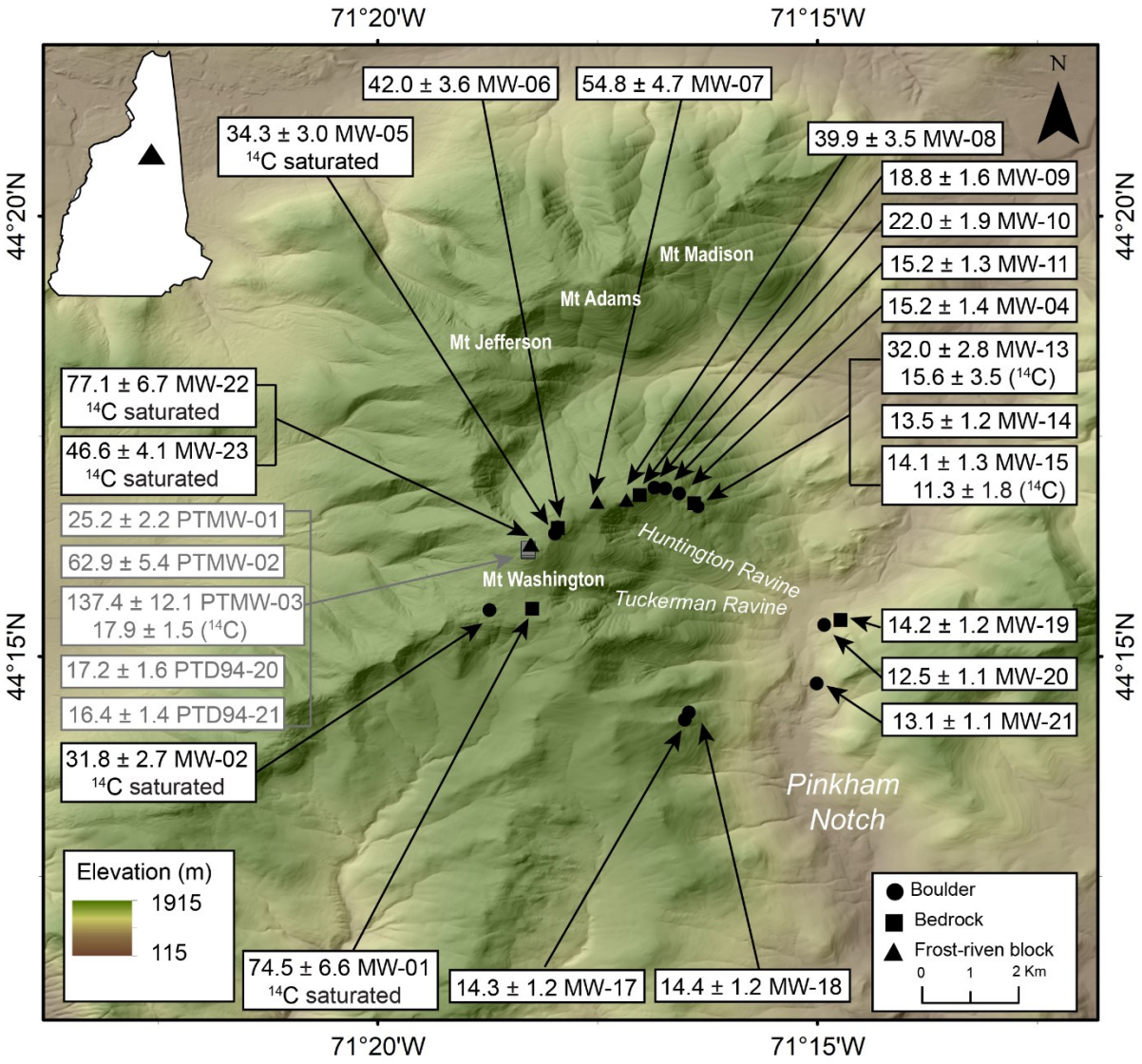
71°20'W
71°15'W
44°20'N
44°15'N
N
42.0 ± 3.6 MW-06
54.8 ± 4.7 MW-07
34.3 ± 3.0 MW-05
14C saturated
39.9 ± 3.5 MW-08
18.8 ± 1.6 MW-09
22.0 ± 1.9 MW-10
15.2 ± 1.3 MW-11
15.2 ± 1.4 MW-04
32.0 ± 2.8 MW-13
15.6 ± 3.5 (14C)
13.5 ± 1.2 MW-14
14.1 ± 1.3 MW-15
11.3 ± 1.8 (14C)
Mt Madison
Mt Adams
Mt Jefferson
77.1 ± 6.7 MW-22
14C saturated
46.6 ± 4.1 MW-23
14C saturated
25.2 ± 2.2 PTMW-01
62.9 ± 5.4 PTMW-02
137.4 ± 12.1 PTMW-03
17.9 ± 1.5 (14C)
17.2 ± 1.6 PTD94-20
16.4 ± 1.4 PTD94-21
31.8 ± 2.7 MW-02
14C saturated
Mt Washington
Huntington Ravine
Tuckerman Ravine
14.2 ± 1.2 MW-19
12.5 ± 1.1 MW-20
13.1 ± 1.1 MW-21
Pinkham Notch
Elevation (m)
1915
115
74.5 ± 6.6 MW-01
14C saturated
14.3 ± 1.2 MW-17
14.4 ± 1.2 MW-18
Boulder
Bedrock
Frost-riven block
0 1 2 Km

725

Figure 3

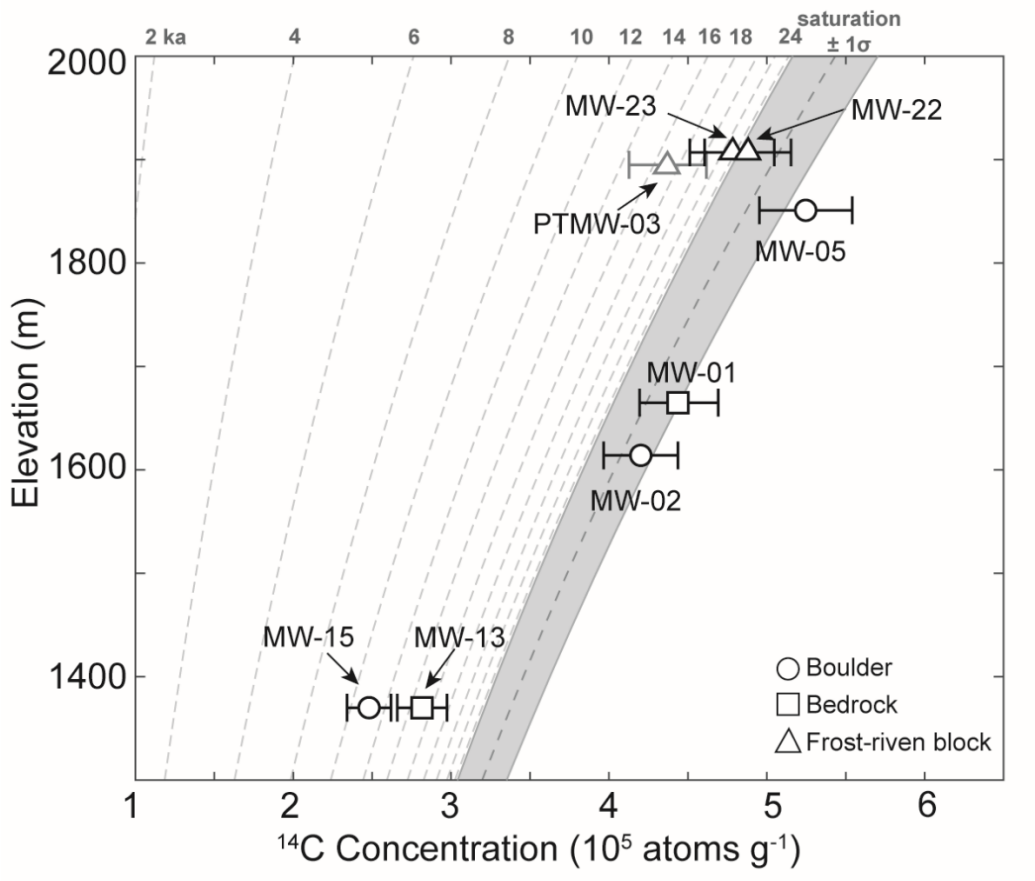

730

Figure 4

735

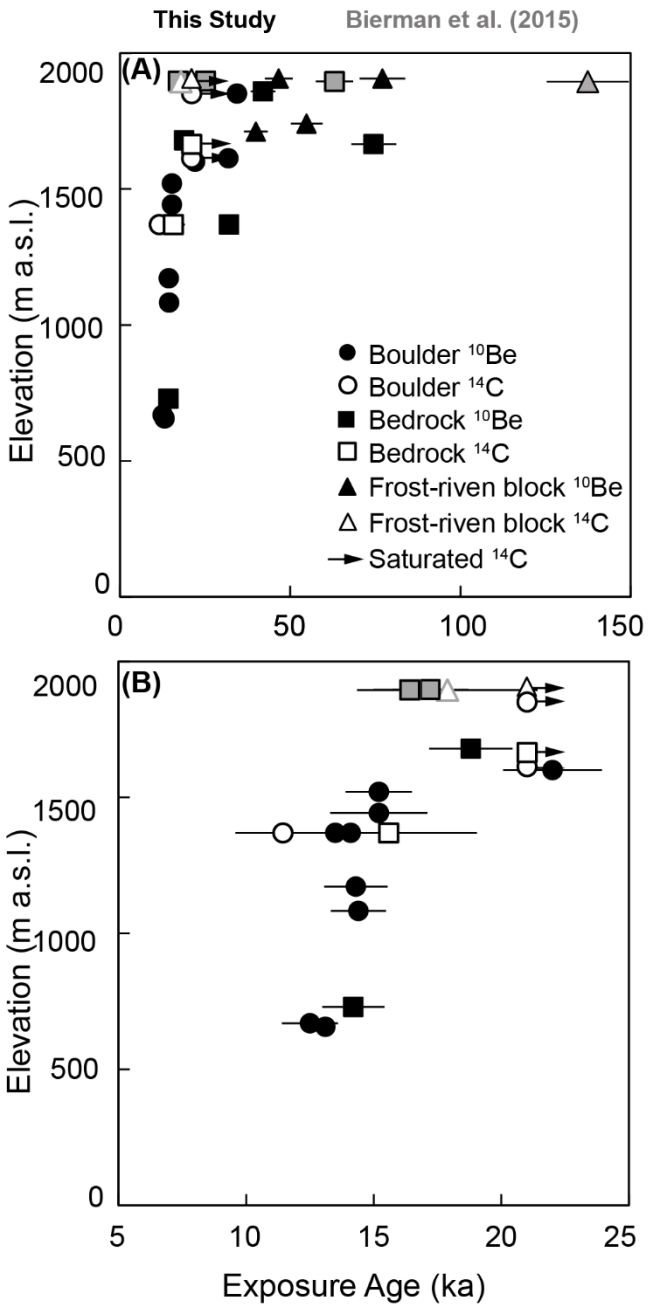
This Study
Bierman et al. (2015)
(A)
(B)
Elevation (m a.s.l.)
Exposure Age (ka)
Boulder 10Be
Boulder 14C
Bedrock 10Be
Bedrock 14C
Frost-riven block 10Be
Frost-riven block 14C
Saturated 14C
0
500
1000
1500
2000
0
50
100
150
5
10
15
20
25

Figure 5

740

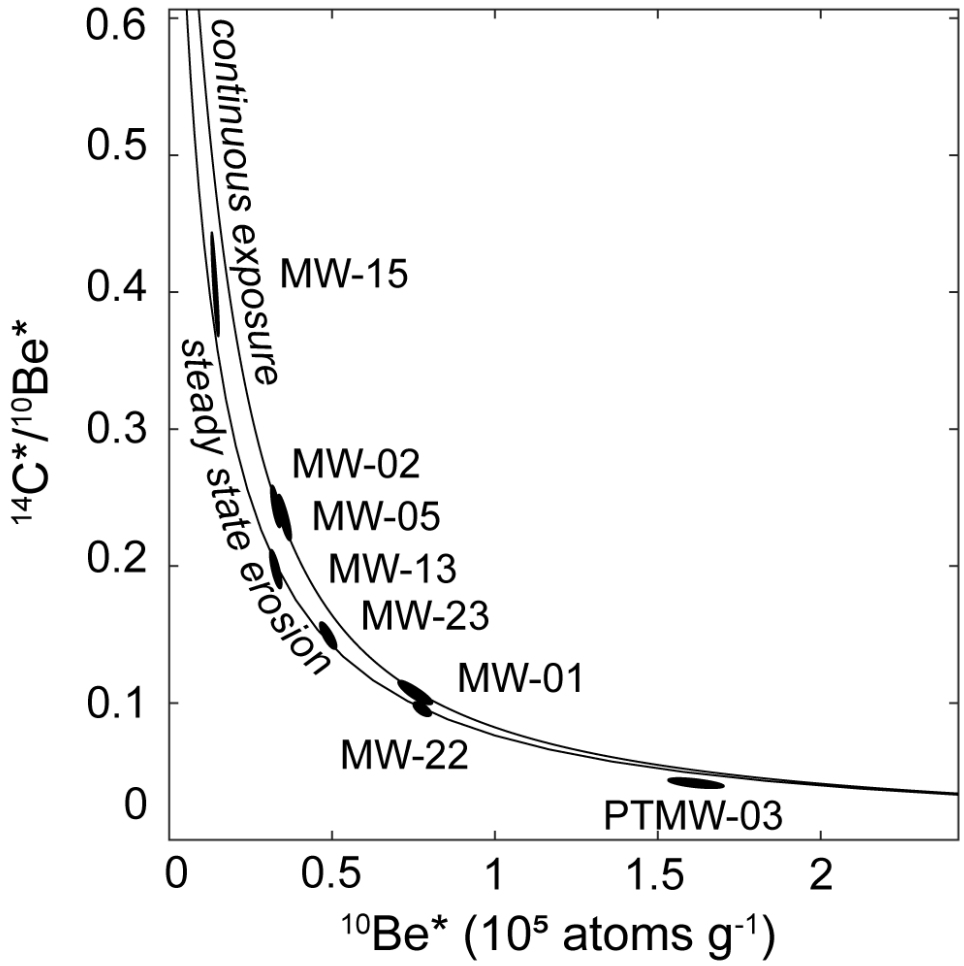
0.6
0.5
0.4
0.3
0.2
0.1
0
$^{14}C^*/^{10}Be^*$
continuous exposure
steady state erosion
MW-15
MW-02
MW-05
MW-13
MW-23
MW-01
MW-22
PTMW-03
0
0.5
1
1.5
2
$^{10}Be^*$ (10^5 atoms g^{-1})

Figure 6

745

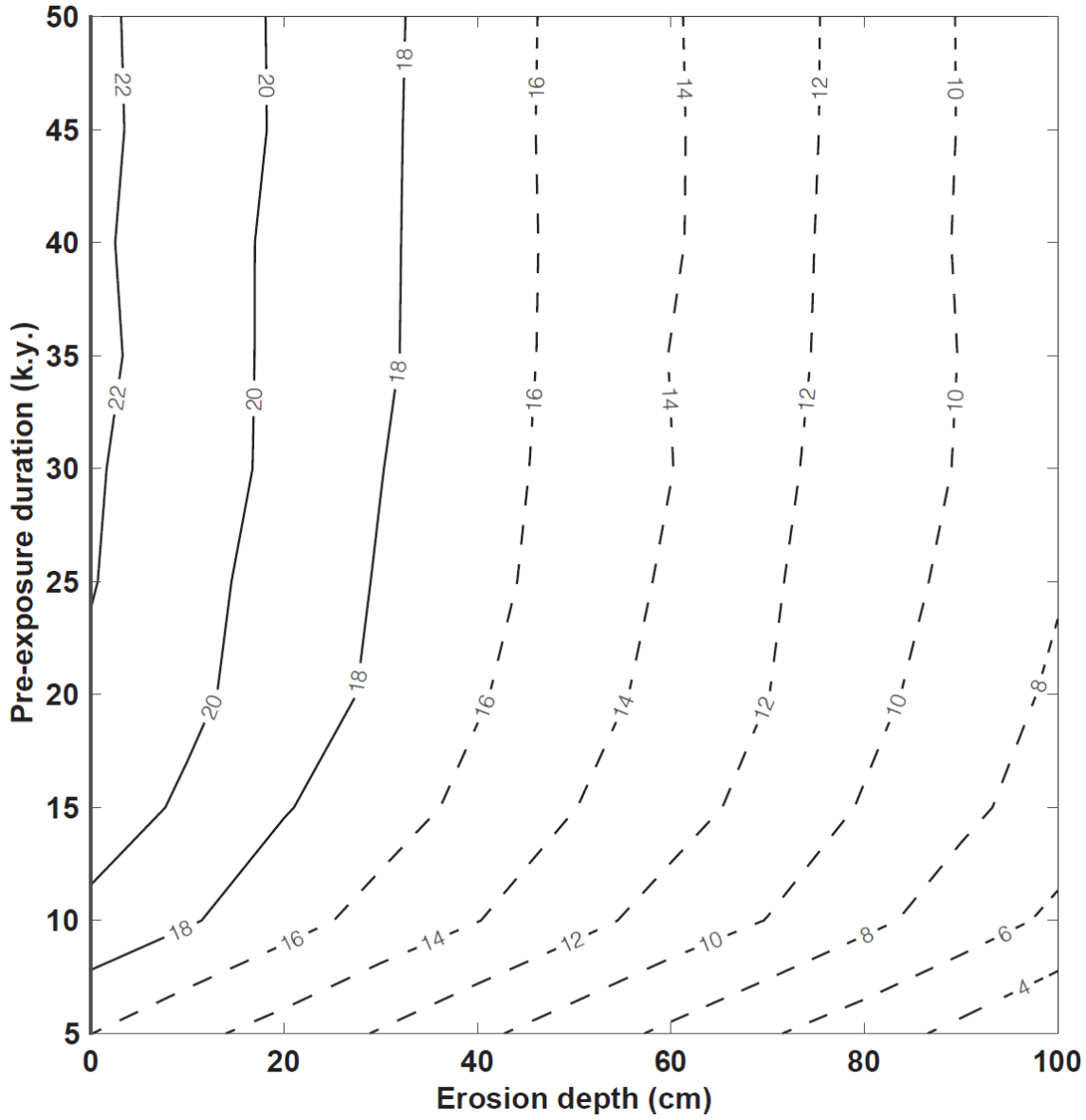
Pre-exposure duration (k.y.)
Erosion depth (cm)
50
45
40
35
30
25
20
15
10
5
0
20
40
60
80
100
22
20
18
16
14
12
10
8
6
4

Figure 7

750

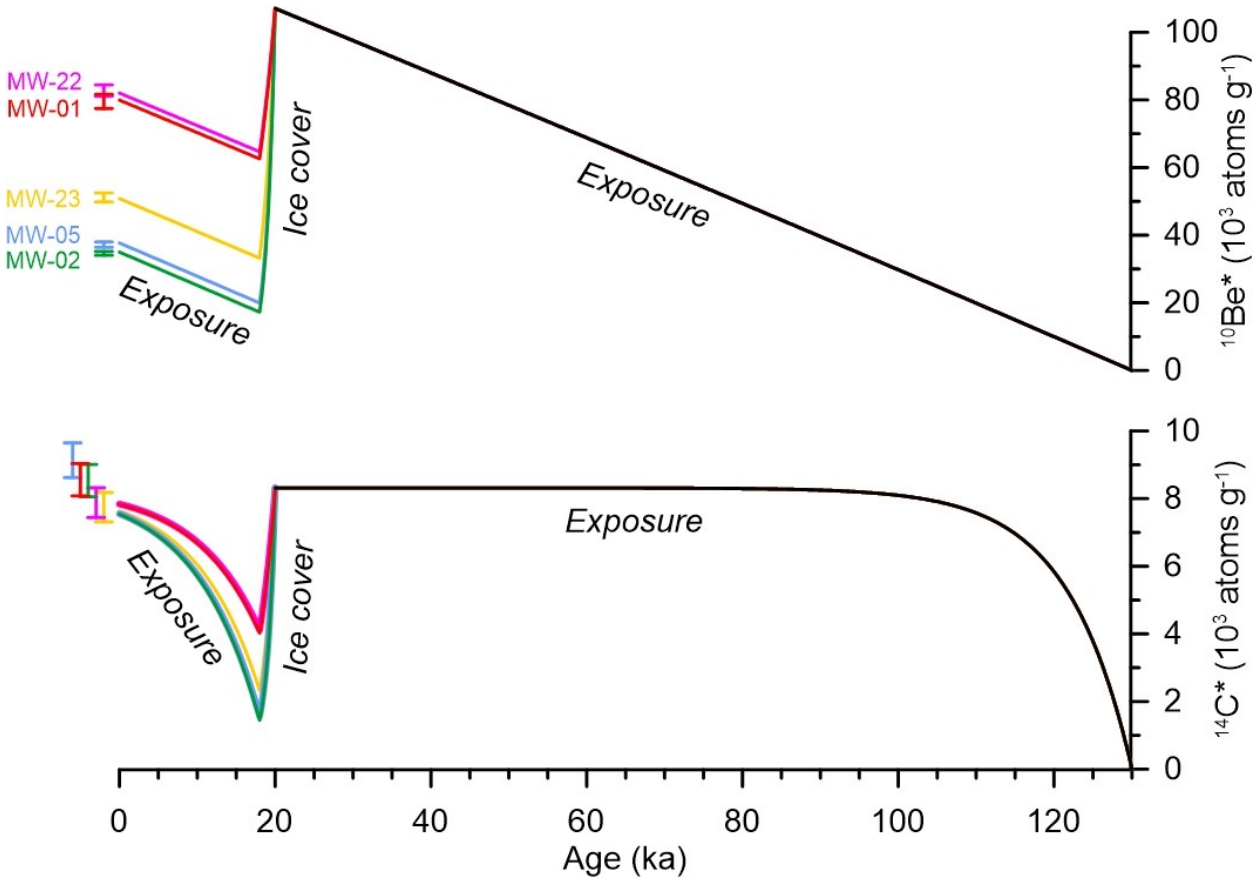

Figure 8

755

760

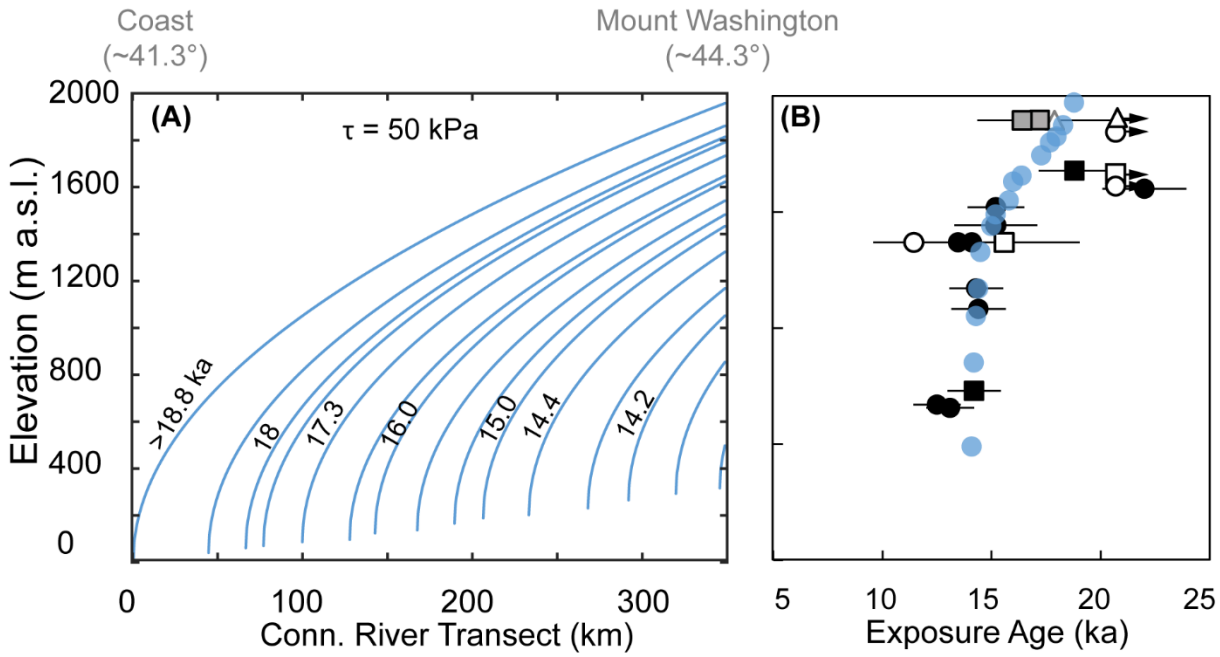
Coast
(~41.3°)
Mount Washington
(~44.3°)
(A)
τ = 50 kPa
(B)
Elevation (m a.s.l.)
2000
1600
1200
800
400
0
>18.8 ka
18
17.3
16.0
15.0
14.4
14.2
0
100
200
300
Conn. River Transect (km)
5
10
15
20
25
Exposure Age (ka)

Figure 9

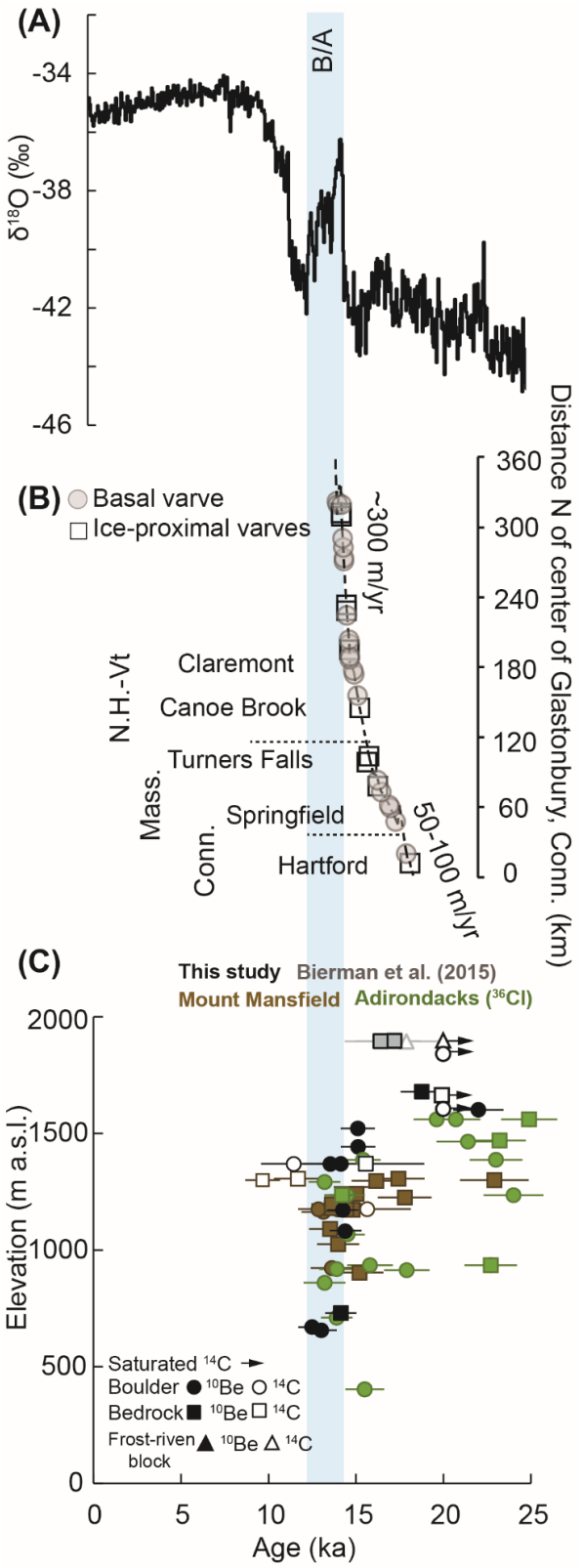

765 **Figure 10**

Table 1: Mount Washington sample locations and field data

Sample Name	Latitude (°N)[a]	Longitude (°E)[a]	Elevation (m a.s.l.)[a]	Type	Sample Thickness (cm)	Shielding[b]	Boulder Height (m)
MW-01	44.25903	-71.30407	1665	Roche Moutonnée	2	1	-
MW-02	44.25879	-71.31216	1614	Boulder	1.5	0.99	1.5
MW-04	44.28087	-71.27620	1443	Boulder	2	0.99	1
MW-05	44.27324	-71.29971	1851	Boulder	1.5	0.99	2.2
MW-06	44.27444	-71.29919	1859	Bedrock	1.5	0.99	-
MW-07	44.27923	-71.29178	1740	Frost-Riven Block	1	0.99	-
MW-08	44.27964	-71.28619	1711	Frost-Riven Block	2.5	0.97	-
MW-09	44.28053	-71.28368	1679	Bedrock	2.5	0.99	-
MW-10	44.28194	-71.28089	1601	Boulder	2	0.99	1
MW-11	44.28183	-71.27884	1521	Boulder	1	0.98	0.8
MW-13	44.27901	-71.27335	1370	Roche Moutonnée	2	0.99	-
MW-14	44.27901	-71.27335	1370	Boulder	1	0.99	0.5
MW-15	44.27901	-71.27335	1370	Boulder	1.5	0.99	0.5
MW-17	44.23803	-71.27509	1172	Boulder	1.5	0.96	2
MW-18	44.23939	-71.27435	1083	Boulder	5	0.95	2
MW-19	44.25686	-71.24559	730	Bedrock	2	0.99	-
MW-20	44.25597	-71.24868	670	Boulder	3	0.98	1
MW-21	44.24489	-71.25013	656	Boulder	2.5	0.97	1.5
MW-22	44.27116	-71.30417	1907	Frost-Riven Block	1.5	1	-
MW-23	44.27117	-71.30450	1907	Frost-Riven Block	1	1	-

[a] Latitude, longitude and elevation were determined with a handheld GPS.

[b] Shielding was calculated with the topographic shielding calculator at http://stoneage.ice-d.org/math/skyline/skyline_in.html.

Table 2: Calculated in-situ ^{10}Be and ^{14}C exposure ages on Mount Washington.

Sample Name	Type	Elevation (m a.s.l.)	^{10}Be Age (ka)[a]	Internal unc (ka)[a]	External unc (ka)[a]	^{14}C Age (ka)[a,b]	Internal unc (ka)[a]	External unc (ka)[a]
MW-22	Frost-Riven Block	1907	77.1	1.6	6.7	29.8	16.5	22.1
MW-23	Frost-Riven Block	1907	46.6	1.2	4.1	25.6	9.8	13.1
MW-06	Bedrock	1859	42.0	0.7	3.6	-	-	-
MW-05	Boulder	1851	34.3	0.7	3.0	saturated	-	-
MW-07	Frost-Riven Block	1740	54.8	0.8	4.7	-	-	-
MW-08	Frost-Riven Block	1711	39.9	0.9	3.5	-	-	-
MW-09	Bedrock	1679	18.8	0.5	1.6	-	-	-
MW-01	Roche Moutonnée	1665	74.5	2.0	6.6	saturated	-	-
MW-02	Boulder	1614	31.8	0.5	2.7	saturated	-	-
MW-10	Boulder	1601	22.0	0.5	1.9	-	-	-
MW-11	Boulder	1521	15.2	0.3	1.3	-	-	-
MW-04	Boulder	1443	15.2	0.5	1.4	-	-	-
MW-13	Roche Moutonnée	1370	32.0	0.7	2.8	15.6	2.6	3.5
MW-14	Boulder	1370	13.5	0.4	1.2	-	-	-
MW-15	Boulder	1370	14.1	0.6	1.3	11.3	1.4	1.8
MW-17	Boulder	1172	14.3	0.3	1.2	-	-	-
MW-18	Boulder	1083	14.4	0.3	1.2	-	-	-
MW-19	Bedrock	730	14.2	0.3	1.2	-	-	-
MW-20	Boulder	670	12.5	0.3	1.1	-	-	-
MW-21	Boulder	656	13.1	0.3	1.1	-	-	-

[a] Exposure ages were calculated with CRONUS-Earth online calculator v. 3 (wrapper script: 3.0.2, constants: 3.0.4, muons: 1A, Balco et al., 2008) using the northeastern North American production rate for ^{10}Be (Balco et al., 2009) and the global production rate for ^{14}C, and the LSDn scaling scheme (Lifton et al., 2014). Ages assume no erosion and a density of 2.7 g cm^{-3}. A spreadsheet of data used to calculate exposure ages is given in Supplemental Table S5.

[b] ^{14}C concentrations within 1σ of saturation are designated saturated.

All uncertainties are 1σ